Proc. Natl. Acad. Sci. USA
Vol. 87, pp. 7570–7573, October 1990
Biophysics

Direct determination of phospholipid lamellar structure at 0.34-nm resolution

(electron microscopy/electron diffraction/direct-phase determination)

DOUGLAS L. DORSET*, ERICH BECKMANN†, AND FRIEDRICH ZEMLIN†

*Electron Diffraction Department, Medical Foundation of Buffalo, Inc., 73 High Street, Buffalo, NY 14203; and †Abteilung Electronenmikroskopie, Fritz-Haber-Institut der Max-Planck-Gesellschaft, Faradayweg 4-6 D1000 Berlin 33, Federal Republic of Germany

Communicated by Herbert A. Hauptman, June 11, 1990 (received for review March 30, 1990)

ABSTRACT **Low-dose, high-resolution electron microscopy combined with conventional direct-phasing methods based on the estimates of triplet-structure invariants are used to determine phase values for all observed electron-diffraction-structure factor magnitudes from epitaxially oriented multilamellar paracrystals of the phosphospholipid 1,2-dihexadecyl-*sn*-glycerophosphoethanolamine. The reverse Fourier transform of these phased-structure factors is a one-dimensional electrostatic potential map that strongly resembles the electron-density maps calculated from similar x-ray-diffraction data. Determination of the phase values for the electron-diffraction data with structure invariants alone is nearly as successful as the combined use of two separate methods, assigning values to 13 of the 16 reflections—i.e., the electrostatic potential map closely resembles the one calculated with all data.**

Several techniques have been used to determine crystallographic phases for x-ray-diffraction data from artificial and natural phospholipid multilamellar arrays. These techniques include sampling the continuous Fourier transform by swelling the multilayers in solvent (1–3), direct deconvolution of the continuous Fourier transform (4, 5), model building (6–8), and interpretation of the Patterson function (6). However, the validity of such structure analyses can be questioned for various reasons. For example, structural rearrangements can occur during solvent swelling (2), if the structure can be swollen at all. Errors propagate in the deconvolution procedure (5) and, furthermore, the *R*-factor figure of merit for an overparameterized fit of a model (9) is imprecise. In this paper we describe a direct determination of phospholipid lamellar structure based on the combined use of high-resolution electron microscope images and Hauptman–Karle three-phase structure-invariant relationships (10) to find phase values for electron-diffraction intensity data, thus overcoming uncertainties encountered in previous analyses.

In the past several years we have demonstrated (11) that it is possible to orient linear chain molecules, including phospholipids, epitaxially on organic substrates by using methods designed originally for linear polymers (12). In the resultant view onto the molecular axis, one can visualize the paracrystalline multilamellar structure directly by low-dose electron microscopy (13). For the example considered here, 1,2-dihexadecyl-*sn*-glycerophosphoethanolamine (DHPE),

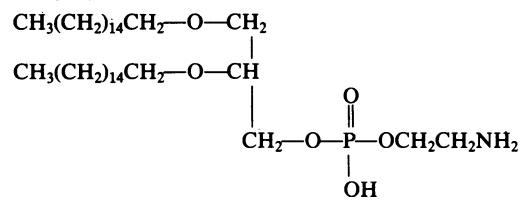

The publication costs of this article were defrayed in part by page charge payment. This article must therefore be hereby marked "*advertisement*" in accordance with 18 U.S.C. §1734 solely to indicate this fact.

as well as other lipid headgroup types (9, 14, 15), it has been possible, moreover, to use the electron-diffraction intensity data (Fig. 1) for quantitative structure analyses. These analyses have been based on a one-dimensional translational search in space group $P\bar{1}$ with models constructed from known x-ray crystal structures, shown by comparison of observed and model Patterson functions to have similar headgroup conformations (6, 16). Although the apparent structural solution for DHPE occurs at a reasonably low minimum of the crystallographic residual (9), the low precision of this figure of merit often does not allow one to identify this solution unequivocally from others indicated by nearby minima. An early use of 1.6-nm resolution lattice images (15), on the other hand, indicated that a more direct phasing procedure may be possible to choose one of several possible model structures.

MATERIALS AND METHODS

Samples of the ether-linked phospholipid DHPE were epitaxially oriented on naphthalene following the technique described earlier (11). After initial nucleation to form thin lath-like crystallites, the nucleating substrate is removed by sublimation *in vacuo*. To obtain the higher-image resolution necessary to phase more of the electron-diffraction intensities, we used the same 100-kV Siemens prototype electron microscope with a liquid-helium-cooled superconducting objective lens that earlier produced 0.25-nm resolution images of solution-grown monolamellar paraffin crystals (17). Typical low-dose techniques were used to minimize radiation exposure to the sample. This involves screening the specimen grid in the electron diffraction mode with very low beam currents (e.g., 10^{-1} e·nm^{-2}·sec^{-1}) to find samples that diffract to suitably high resolution. When a satisfactory microcrystalline area is found, the beam is deflected to a nearby area to allow final adjustments to be made at a higher current in the image mode for astigmation and focus. The final exposure is taken at lower beam current, so that the total dose to the specimen at ×66,000 direct magnification is ≈1000 e·nm^{-2}.

Electron micrographs are next placed on an optical bench to find image areas that diffract to high resolution. After these areas are identified, they can be converted to a digitized array with a rotating drum microdensitometer, such as an Optronics P1000. For our instrument, the smallest raster size available is 25 μm. As will be discussed below, this digital image file can be manipulated with image-processing computer software to determine the crystallographic phases of the 00*l* diffraction spots via a computed Fourier transform.

Electron diffraction experiments were carried out at 100 kV with a JEOL JEM-100B7 electron microscope, also taking care to minimize the electron-beam dose to the sample (at room temperature) by reducing the incident beam current and by use of a photographic film (Kodak DEF-5 x-ray film) that

Abbreviation: DHPE, 1,2-dihexadecyl-*sn*-glycerophosphoethanolamine.

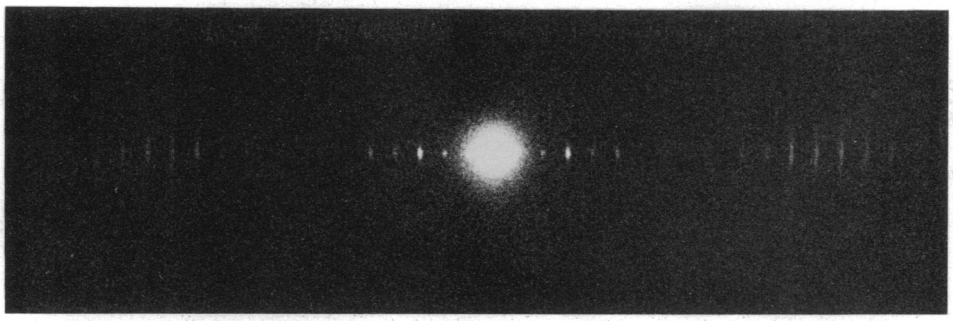

FIG. 1. Electron diffraction pattern from DHPE crystallized on naphthalene. The lamellar spacing is 5.52 nm. Note that an alternation of strong and weak reflections is found for the low-angle-diffraction maxima and a zone of reflections with intensities within a Gaussian envelope is seen at wider angles.

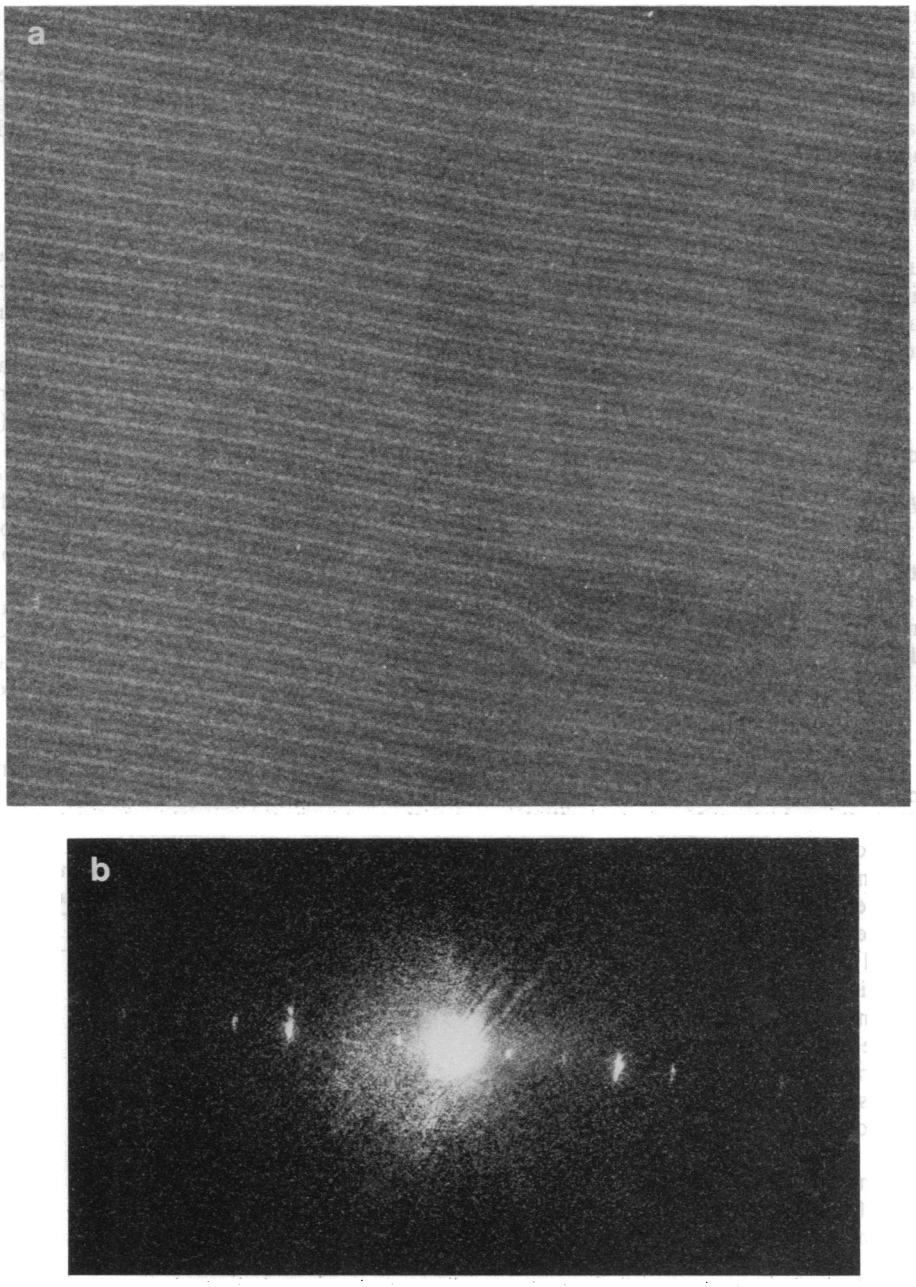

FIG. 2. (*a*) High-resolution electron microscope image of DHPE obtained at 100 kV with the Suleika electron microscope with ×66,000 direct magnification on Agfa 23D56 film and total radiation exposure of 1000 e·nm^{-2}. The specimen temperature was near 4 K. With the spherical aberration constant C_s = 1.35 mm and a defocus value near −282.8 nm, the computed phase-contrast transfer-function envelope changes sign at (1.0 nm)$^{-1}$. As shown by comparing Fourier transform magnitudes computed from similar images of *n*-hexatriacontane to their electron-diffraction-structure factor magnitudes (see ref. 21), the actual contrast-function envelope is found in many of our images to have its first zero near (0.92 nm)$^{-1}$ (lamellar repeat, 5.52 nm). (*b*) Optical transform of a DHPE low-dose electron microscope image. Note similarity of low-angle reflection intensity to the electron diffraction pattern in Fig. 1.

Table 1. Phase assignments for DHPE from electron image and use of direct methods

Electron microscopy	Direct methods (three-phase structure invariants)
$\phi_{001} = \phi_{003} = \phi_{005} = 0$	Origin definition $\phi_{001} = 0$
$\phi_{002} = \phi_{004} = \phi_{006} = \pi$; $\phi_{007} = \pi$	Sigma 2 invariants ordered according to value of $A_2 = k\lvert E_{\mathbf{h}_1} E_{\mathbf{h}_2} E_{\mathbf{h}_3}\rvert$ $\phi_{00,10} = \phi_{00,11} = \phi_{00,12} = \phi_{00,13} = \phi_{00,14} = \phi_{00,15} = \phi_{00,16} = a$; $\phi_{003} = 0$ Sigma 1 invariants with predicted value of π according to $A_1 = (\lvert E_{\mathbf{h}}\rvert^2 - 1)\lvert E_{2\mathbf{h}}\rvert/\sqrt{N}$ $\phi_{002} = \phi_{004} = \phi_{006} = \phi_{008} = \phi_{00,10} = \pi$ thus $a = \pi$
	$\phi_{009} = \pi$ estimated from numerous triple relationships with lower A_2 value

is sufficiently sensitive at the desired magnification of the diffraction pattern. The intensities of the diffraction spots were obtained by scanning the films on a Joyce Loebl MkIIIC flat-bed microdensitometer and then integrating the peak area. As discussed earlier (9), an effective Lorentz correction is needed, accounting for the arcing of the spots (Fig. 1). This correction merely multiplies the intensity of a peak I_{obs} by the order to the diffraction peak l. The relevance of other errors (e.g., due to n-beam dynamical scattering) to the accuracy of the intensity measurement was discussed earlier (9). An additional perturbation due to incoherent multiple scattering has been detected and will be reported subsequently (18). After determining the observed structure factor magnitude by

$$|F^{00l}_{obs}| = (I^{00l}_{obs} \cdot l)^{1/2}, \quad [1]$$

the normalized structure factor $|E_{obs}|$ is found by

$$|E^{00l}_{obs}|^2 = |F^{00l}_{obs}|^2 / \sum_i f_i^2, \quad [2]$$

where f_i is the scattering factor (19) of atom i, assuming thermal vibrations to be absent. The values of $|F|$ were originally placed on an absolute scale by reference to a packing model based on a similar crystal structure (see ref. 9). As usual (10), the $|E|$ values are scaled by specifying that $\langle |E|^2 \rangle = 1.0$.

RESULTS

Initial low-dose experiments on epitaxially crystallized n-hexatriacontane (20) indicated that the most radiation-sensitive $00l$ row of reflections could be directly observed at least to 0.5-nm diffraction resolution, as shown in the optical transform of the experimental phase-contrast microscope image. Similar quality images were obtained from the phospholipid (Fig. 2*a*). (It should be emphasized that these preparations are not fixed or stained or treated in any way.) Optical transforms (Fig. 2*b*) sometimes reveal a 0.6-nm diffraction resolution in these images. They also show directly that the arc-like trace of the diffraction spots is due to a curvilinear lamellar disorder. This distortion can be removed by selection of small areas which, upon image analysis via Fourier peak-filtration techniques (22), can be used to determine crystallographic phases after the image is shifted to an allowed unit cell origin. The phases of the first seven lamellar reflections in the computed Fourier transforms, listed in Table 1, are found to correspond to the values determined in the earlier structural analysis with a molecular model (9).

Phase extension to higher resolution is achieved by use of three-phase structure invariants (10) in space group $P\bar{1}$. Assuming the periodic bilayer profile (repeat distance = 5.52 nm) to be centrosymmetric, the $00l$ phases can be restricted to the values 0 or π. The value of a linear combination of phases (so-called sigma 2 triples):

$$\psi = \phi_{\mathbf{h}_1} + \phi_{\mathbf{h}_2} + \phi_{\mathbf{h}_3}, \text{ where } \mathbf{h}_1 + \mathbf{h}_2 + \mathbf{h}_3 = 0 \quad [3]$$

is estimated according to the magnitudes of the normalized electron-diffraction structure factor amplitudes $|E_{\mathbf{h}}|$, calculated from $|F_{\mathbf{h}}|$ in the usual way (23). In addition, the so-called sigma 1 relationships:

$$\psi = \phi_{\mathbf{h}} + \phi_{\mathbf{h}} + \phi_{-2\mathbf{h}}, \quad [4]$$

can be used to identify reflections for which $\phi_{2\mathbf{h}} = \pi$. (10). Specifying the phase of one reflection—e.g., $\phi_{001} = 0$, to define the origin (by necessity, in agreement with the origin defined from the electron microscope images), the most probable sigma 2 invariants can be evaluated. From these phase relationships, a group of reflections at higher angles is shown to have the same phase value (Table 1). From the sigma 1 triples, this group of reflections is found to have the phase value π, as are the phases of several other low-angle reflections, some of which can be verified by phase determination from the electron microscope image (Table 1). Thus, 15 of 16 reflections are assigned phase values, leaving one, ϕ_{009}, from a weaker reflection that is somewhat uncertain. However, if one looks at the next group of triple relationships below the probability threshold where the first phase error was detected, it is found that relationships were $\phi_{009} = \pi$ occur more frequently than ones where a 0 value is assigned.

The phase assignment is in complete agreement with the earlier structure determination based on a molecular model (9), as can be seen by the comparison of Table 2. A one-dimensional electrostatic-potential map generated from the

Table 2. Comparison of phase assignments for electron diffraction data from epitaxially crystallized DHPE

l	$\lvert E_{obs}\rvert$	ϕ_m	ϕ_{I+DP}	ϕ_{DP}
1	0.920	0	0	0
2	0.469	π	π	π
3	0.964	0	0	0
4	0.547	π	π	π
5	0.722	0	0	—
6	0.434	π	π	π
7	0.591	π	π	—
8	0.165	π	π	π
9	0.523	π	π	—
10	0.836	π	π	π
11	0.932	π	π	π
12	1.524	π	π	π
13	1.513	π	π	π
14	1.554	π	π	π
15	1.486	π	π	π
16	1.244	π	π	π

ϕ_m, Determination with molecular packing model (ref. 9); ϕ_{I+DP}, determination with images and direct phasing; ϕ_{DP}, determination with direct phasing alone.

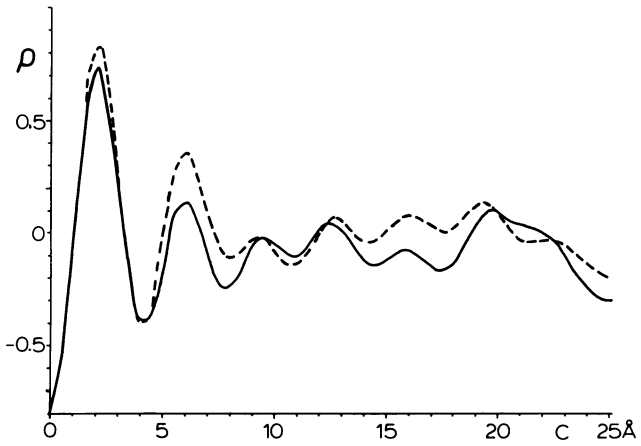

FIG. 3. One-dimensional electrostatic-potential map (one-half of the phospholipid bilayer) calculated with the 16 phased electron-diffraction-structure factors (for values, see ref. 9) is shown by the unbroken line; the calculation is on a relative scale. An electrostatic-potential map calculated with 13 of the 16 data phases by direct methods alone is plotted by the broken line.

phased-structure factors is shown in Fig. 3. Although the phases determined from high-resolution electron images are certainly useful for establishing the correctness of the low-angle phases obtained from triple-phase relationships, it is interesting to note what happens if only the electron diffraction data themselves are used, so that only one phase—e.g., $\phi_{001} = 0$—is specified initially for origin definition. By using the outline in Table 1, the values of ϕ_{005} and ϕ_{007} are found to be ambiguous in addition to ϕ_{009}; that is to say, 13 of 16 observed reflections can be phased *ab initio* by using structure-invariant relationships. The resulting electrostatic-potential map is not greatly different from the one calculated from all the phased data.

DISCUSSION

It is evident, from the above analysis, that molecular models are not necessary for determining one-dimensional lipid packings from experimental diffraction data, thus eliminating the uncertainties inherent in the use of crystallographic residuals as a figure of merit. The advantage of the direct-phasing methodology is that is can be used for lamellar structures for which the continuous Fourier transforms cannot be sampled by swelling in a solvent. The catalog of lipid structures which can be epitaxially crystallized to provide a view onto the lamellae, as shown in Fig. 2, is rather large (11) and includes headgroup classes for which no x-ray crystal structures are currently available. It is, therefore, envisioned that a similar combination of electron microscope images with crystallographic direct-phase determination will readily provide a facile comparison of previously uncharacterized lamellar structures with known structures to ascertain when the molecular packing arrangements are similar. The unexpected success of the direct-phasing method by itself indicates that it may also be applied to x-ray data from multilamellar arrays of phospholipids built up, e.g., by repeated dippings of a flat substrate through a Langmuir–Blodgett monolayer film (18).

1. Worthington, C. R. & McIntosh, T. J. (1973) *Nature (London) New Biol.* **245**, 97–99.
2. Torbet, J. & Wilkins, M. H. F. (1976) *J. Theor. Biol.* **62**, 447–458.
3. McIntosh, T. J. (1980) *Biophys. J.* **29**, 237–245.
4. Worthington, C. R., King, G. I. & McIntosh, T. J. (1973) *Biophys. J.* **13**, 480–494.
5. Worthington, C. R. & Khare, R. S. (1978) *Biophys. J.* **23**, 407–425.
6. Khare, R. S. & Worthington, C. R. (1978) *Biochim. Biophys. Acta* **514**, 239–254.
7. Hitchcock, P. B., Mason, R. & Shipley, G. G. (1975) *J. Mol. Biol.* **94**, 297–299.
8. Wiener, M. C., Suter, R. M. & Nagle, J. F. (1989) *Biophys. J.* **55**, 315–325.
9. Dorset, D. L., Massalski, A. K. & Fryer, J. R. (1986) *Z. Naturforsch. A.* **42**, 381–391.
10. Hauptman, H. & Karle, J. (1953) *Solution of The Phase Problem I: The Centrosymmetric Crystal* (Edwards Brothers, Ann Arbor, MI).
11. Dorset, D. L., Pangborn, W. A. & Hancock, A. J. (1983) *J. Biochem. Biophys. Methods* **8**, 29–40.
12. Wittmann, J. C. & Manley, R. St. J. (1978) *J. Polym. Sci. Polym. Phys. Ed.* **16**, 1891–1895.
13. Fryer, J. R. & Dorset, D. L. (1987) *J. Microsc. (Oxford)* **145**, 61–68.
14. Dorset, D. L. (1987) *Biochim. Biophys. Acta* **898**, 121–128.
15. Dorset, D. L. (1988) *Biochim. Biophys. Acta* **938**, 279–292.
16. Dorset, D. L. (1987) *J. Electron Microsc. Tech.* **7**, 35–46.
17. Zemlin, F., Reuber, E., Beckmann, E., Zeitler, E. & Dorset, D. L. (1985) *Science* **229**, 461–462.
18. Dorset, D. L. (1990) *Biophys. J.*, in press.
19. Ibers, J. A. & Hamilton, W. C. (1974) *International Tables for X-Ray Crystallography* (Kynoch, Birmingham, England), Vol. 4, p. 155.
20. Dorset, D. L., Holland, F. M. & Fryer, J. R. (1984) *Ultramicroscopy* **13**, 305–310.
21. Unwin, P. N. T. & Henderson, R. (1975) *J. Mol. Biol.* **94**, 425–440.
22. Heel, M. V. & Keegstra, W. (1981) *Ultramicroscopy* **7**, 113–130.
23. Dorset, D. L. & Hauptman, H. (1976) *Ultramicroscopy* **1**, 195–201.